Journal of Harbin Engineering University Vol 44 No. 7
ISSN: 1006-7043 July 2023

ORSAN: A ResNet-based Model Optimized for COVID-19 Diagnosis using X-ray Images

Jaswinder Singh[1,2], Dr. B. K. Sharma[3]
[1]Research Scholar, Dr. A. P. J. Abdul Kalam technical University, Lucknow
[2]Department of Information Technology, KIET Group of Institutions, Delhi-NCR, Ghaziabad, India
[3]Principal Scientific Officer and Head Computer Science and Engineering Department, NITRA Technical Campus, Ghaziabad

Abstract. The use of deep learning (DL) models for analysing X-ray pictures in the context of novel coronavirus illness (COVID-19) is the main topic of this research. By simply replacing spatial convolutions with global self-attention in the final three bottleneck blocks of a ResNet, a unique DL technique known as ORSAN is created. A dataset of 5,935 X-ray images gathered from publically available datasets is used to train and assess the ORSAN. Different assessment metrics are utilised to evaluate the model's performance, including classification accuracy, F1 score, recall, precision, and area under the receiver operating characteristics curve (AUC). Preprocessing techniques including resizing, augmentation, and normalisation are used. The experimental findings show that the ORSAN consistently performs the best when classifying X-ray pictures into three groups: healthy lungs, lungs affected by pneumonia, and lungs affected by COVID-19. When utilising ResNet101 as the foundation, the detection accuracy for COVID-19 is 98.74%, and for healthy lungs and lungs damaged by pneumonia, it is 92.08% and 91.32%, respectively. Additionally, using the ResNet152 backbone, accuracy values of 83.68% and 82%, respectively, are obtained for healthy lungs and lungs afflicted by pneumonia. These results demonstrate the possibility of the proposed ORSAN model for precise COVID-19 and pneumonia case classification using X-ray images.

Keywords: COVID-19, coronavirus, deep learning, X-ray, ResNet, ORSAN

1. Introduction

Since December 2019, the novel coronavirus illness (COVID-19) has been causing a global pandemic that has affected a number of nations [2,3]. COVID-19 has been linked to symptoms like cough, fever, dyspnea, sore throat, and pneumonia [4]. Chest X-ray imaging can be used to detect the condition, which frequently manifests as pneumonia or a lung infection [5,6]. Therefore, it is essential to get an early and precise diagnosis in order to stop the infection from spreading. An effective defence against COVID-19 is the identification of coronavirus infection [8, 62, 64]. Numerous nations have recently seen the second wave of the viral outbreaks, which have resulted in rising daily infection and mortality rates [9,10]. However, there are a number of drawbacks to the present approaches for COVID-19 early detection and management. To battle the disease, researchers from all around the world are actively striving to create efficient therapies, vaccinations, and diagnostic methods.The three primary methods for diagnosing COVID-19 are viral tests, medical imaging, and blood tests [11]. The severe acute respiratory syndrome coronavirus type 2 (SARS-CoV-2) antibodies can be found through blood tests [12]. Viral testing can also be used to find coronavirus antigens [13]. Diagnose COVID-19 and treat its lung-damaging effects with the help of medical imaging, such as chest X-rays or CT scans [14,15]. In order to stop the transmission of the virus and lessen its effects on public health, these diagnostic techniques are essential for the early detection and therapy of COVID-19. For the detection of COVID-19, viral tests like reverse transcription polymerase chain reaction (RT-PCR) are frequently utilised. However, studies have revealed that RT-PCR's sensitivity is just 50 to 62%, indicating probable errors. It may also take longer to get data. Multiple tests are frequently needed as a result to obtain reliable results. In some nations, the availability of RT-PCR assays may also be constrained, leading to expensive diagnoses for patients or healthcare authorities. As a result, new techniques for COVID-19 detection are required.SARS-CoV-2, the virus that causes COVID-

19, can be found utilising imaging techniques like X-ray, ultrasound, or computed tomography (CT) scan with the help of artificial intelligence (AI). For the diagnosis of lung disorders, such as pneumonia and viral or bacterial infections, chest X-rays or CT scans are frequently employed. While RT-PCR can provide precise details on the existence of the coronavirus, it might not be able to provide light on other lung diseases such pneumonia or pulmonary fibrosis. Therefore, it is essential to use chest imaging methods to assess the degree of lung involvement in COVID-19 cases. However, X-rays and CT scans may have drawbacks as well, such as occasionally producing false-negative results. Many research have documented the use of CT scans and X-ray images in the early diagnosis of COVID-19 even before symptoms manifest, and some studies have demonstrated that CT scans may have greater sensitivity than RT-PCR. Although X-ray devices are more readily available in underdeveloped nations and are frequently used for analysing various infections, CT scans may not be broadly accessible or may be expensive in some circumstances. A growing number of diseases, such as breast cancer, brain tumors, gastric cancer, lung cancer, skin conditions, and skin cancer, can now be detected and diagnosed using computer-aided diagnosis (CAD) techniques that use deep learning (DL) and artificial intelligence (AI). The ability of DL models, like NASNet, to correctly identify COVID-19 patients from CT scan pictures has showed promise. In the context of the COVID-19 pandemic, where there may be a lack of radiologists relative to the enormous number of infected patients, the incorporation of AI-based diagnosis tools can help radiologists achieve correct diagnoses in a timely manner. Optimized residual networks are used in the proposed DL-based model, known as ORSAN, to analyse chest X-rays from COVID-19 patients, pneumonia cases, and healthy lungs. 5,935 chest X-ray pictures from the experiment's dataset were split into training and testing samples using the holdout method. RT-PCR is a typical viral test for detecting COVID-19, however it has drawbacks in terms of producing results quickly and having a chance of being inaccurate. In situations where RT-PCR testing may be expensive or seldom available, imaging methods like X-rays and CT scans paired with AI-based diagnosis algorithms can offer helpful insights in the early detection and correct diagnosis of COVID-19 patients. With the potential to help radiologists correctly diagnose infectious lung disorders like COVID-19, the suggested ORSAN model provides a potential solution for examining chest X-ray pictures for pneumonia, normal lungs, and COVID-19.

2.Background

Deep learning (DL) and X-rays have been discussed extensively in the context of the identification and diagnosis of COVID-19. In this section, certain noteworthy studies are highlighted.In a recent work [34], a model named COVIDX-Net was created, and for binary classification, a comparison of different deep learning (DL) models including ResNetV2, VGG19, InceptionV3, DenseNet201, MobileNetV2, Xception, and InceptionResNetV2 was done. 50 X-ray samples total were used in the investigation, 25 of which were classified as COVID-19 positive and 25 as normal [34]. The accuracy results were compared with data from another source [36] and two other databases of COVID-19 X-ray images [35], which had 123 X-ray images of the lung's anterior view. In this investigation, DenseNet201 and VGG19 both had 90% accuracy [34]. However, the tiny dataset employed in this study constituted one of its limitations.

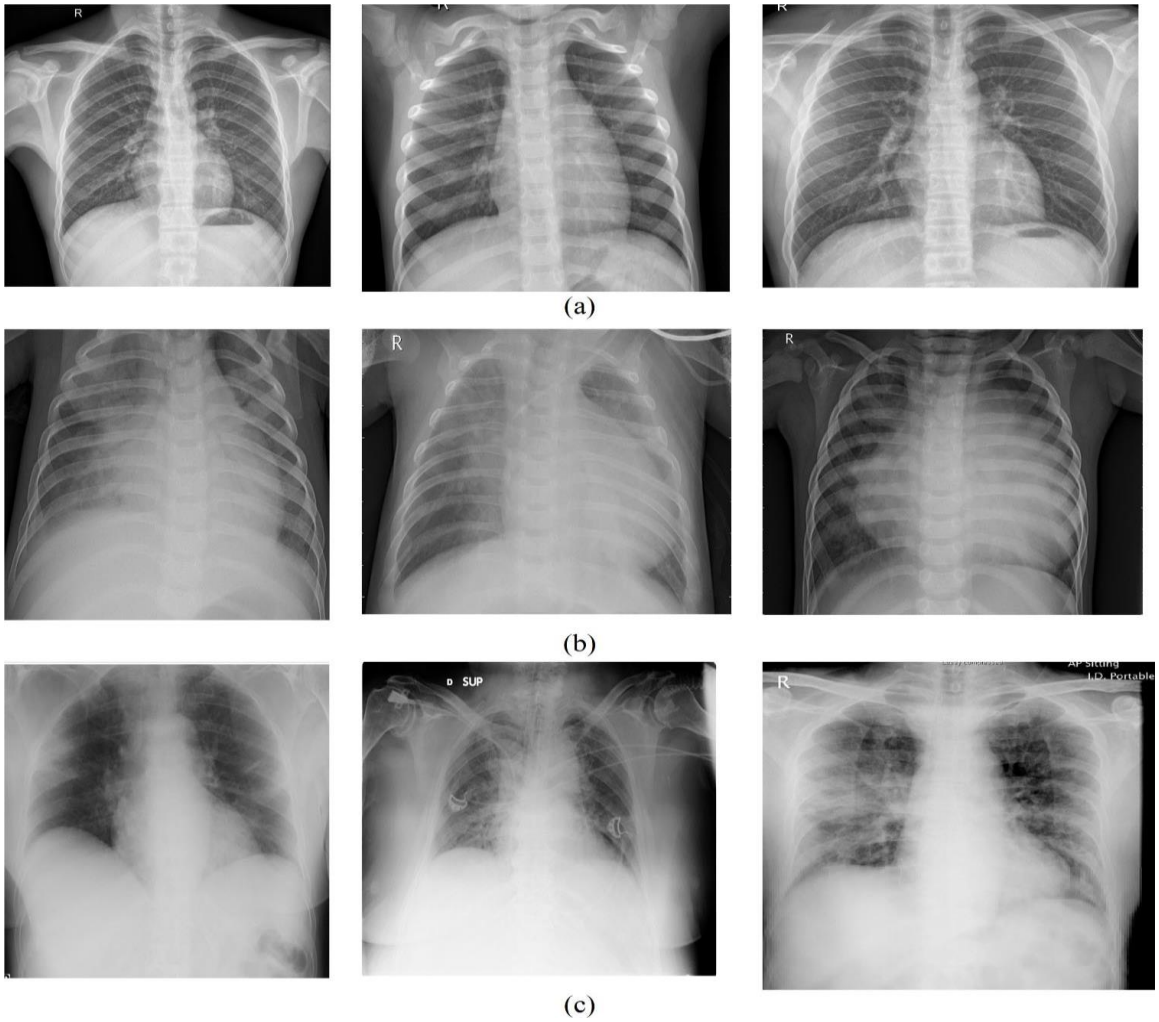

Fig. 1. Example of the (a) normal, (b) pneumonia, and (c) COVID-19 experimental X-ray images [65].

Similar to this, ResNet50 and VGG19 models were used in a different study [37] to compare the outcomes with the COVID-Net model. For the classification of multiclass data, including pneumonia, COVID-19, and normal patients, the study used a pre-trained ImageNet with Adam optimizer. The accuracy achieved, at 93.3%, was higher than in the earlier trial. 13,975 X-ray pictures from various sources [35, 38–41] made up the dataset used in this work. Data augmentation techniques were used to solve the issue of an unbalanced dataset. The dataset for a second study [42] that also used the VGG19 model was obtained from Ref [35, 39], SIRM [43], and Radiopaedia [44], among other sources. The collection included 224 COVID-19 pictures, 504 normal photos, and 700 images of pneumonia. Both multi-class and binary classification experiments were done, and multi-class classification had an accuracy of 93.48% while binary classification had a peak accuracy of 98.75% [42]. Previous research [34, 37] shown that VGG19 offered more accurate findings when compared to other models. SVM and ResNet50 were used in a different work [45] to classify COVID-19 using X-ray pictures. A total of 50 chest X-ray images were employed for the study's experimental purposes, and they were gathered from two separate databases: Kaggle [46] and Cohen [35]. An accuracy of 95.38% for binary classification was attained in the study by the authors in [45], outperforming the outcomes found in the work [34]. The authors presented DarkNet, a different suggested model, in [47]. For COVID-19 diagnosis using X-ray pictures, this study used two datasets, [34,47], for both multiclass (500 no-findings, 500 pneumonia, and 124 COVID-19) and binary (500 no-findings and 125 COVID-19) classifications. The DarkNet model had a leaky ReLu activation function and 17 convolution layers. For multiclass

classification, accuracy was 82.02%, and for binary classification, accuracy was 98.08% [47]. A modified Unet model was suggested and results with and without segmentation were provided in a distinct investigation by the authors in [51]. They used 18,479 X-ray images in total, 3,616 of which were of individuals who had the COVID-19 virus. The photos were acquired from two different databases, and the lungs were divided into three groups: lungs in good health, lungs with lung opacity, and lungs with COVID-19 infection [51]. These models have some drawbacks in addition to their advantages in the COVID-19 diagnosis using X-ray pictures. As a result, we suggest using ORSAN algorithms as a substitute strategy. Binary classification had an accuracy of 98.75%, while multi-class classification had an accuracy of 93.48%. [43].

Table 1.Brief of literature reviews

Modalities	Images	Model	Evaluation matrices	Ref
X-ray	50	COVIDX-Net	Precision: 83%, F1-Score: 91%, recall: 100%, accuracy: 90%	[33]
	13,975	COVID-Net	Accuracy: 93.3%	[36]
	1,428	VGG19	Accuracy: 93.48%	[41]
	50	ResNet50	Accuracy: 95.38%	[44]
	1124	DarkNet	Accuracy: 82.02%	[46]
	18479	Modified unet	Sensitivity: 97.28%, F1-score: 96.28%, accuracy: 96.29%,	[50]
	284	nCOVnet	AUC: 88%, Accuracy: 88.10%	[51]
	5,310	Deep Bayes-SqueezeNe	Accuracy: 98.26%	[52]
	3,487	DenseNet201, AlexNet, SqueezeNet, ResNet18	Accuracy: 97.94%	[53]

Table 2.. Summary of dataset splitting into training 80% and testing 20%

Class	Training images	Testing images
0: Normal	1263	320
1: Pneumonia	3426	847
2: COVID-19	59	20
Total:	4748	1187

3.Data availability

Two separate open access sources provided the experimental data for this investigation. From the database of [46], chest X-ray images of healthy people and patients with pneumonia were extracted, with 1,583 photos of healthy lungs and 4,273 images of patients with pneumonia. In addition, 79 chest X-rays from another dataset of [49] that had COVID-19-affected photos were gathered. The collection included 5,935 X-ray pictures in total. The dataset was then divided into 20% for testing and 80% for training. The experimental dataset is summarised in Table 2, and a sample dataset is shown in Fig. 1.

4. Methodology

With Multi-Head Self-Attention (MHSA) levels that carry out global (all2all) self-attention throughout a 2D feature map, we swap out the final three spatial (3x3) convolutions in a ResNet (as illustrated in Fig. 4). ResNet typically has four stages (or module groups): [s2, s3, s4, s5] with relative strides of [4, 8, 16, 32]. Approaches that make use of self-attention across the backbone [1], [1] are practical at input resolutions of 224 x 224 (for classification) and 640 x 640 (for detection experiments in SASA [1]).

But since larger-resolution images (1024 x 1024) are frequently employed in high-performance

instance segmentation approaches, our aim is to apply attention in more realistic settings. The simplest configuration that satisfies the aforementioned requirements, in our opinion, is to incorporate self-attention at the lowest pixel density feature maps in the backbone, specifically the residual modules in the s5 stack. This is because self-attention across n entities requires O(n2*d) space and computation [1]. The s5 stack in a ResNet backbone typically consists of three blocks with a spatial 3x3 convolution in each block. The MHSA layers in the BoTrNe architecture are intended to take the role of these blocks. A 3x3 convolution with a stride of 2 is used in the first block of the s5 stack, while a stride of 1 is used in the remaining two blocks. We use a 2x2 mean with a stride of 2 for the first BoTr block because all2all attention isn't really a strided operation[1]. We carried out our experiments in stages. First, we performed normalisation and scaling of by-ray pictures to 224 by 224 pixels in order to aid with data generalisation. The dataset was then further augmented using data augmentation techniques. The experimental dataset was then split into testing and training portions, as shown in Table 2. We experimented for up to 30 epochs after using our ORSAN model to train our data. Within 30 epochs, our ORSAN model had reached its highest level of accuracy. After that, we adjusted our model's hyperparameters. Various performance measures were used to analyse the entire system.

5. Experimental Results

Using Google Colaboratory, commonly known as Colab, a cloud-based open-source platform that offers Jupyter notebook for deep learning, the tests and findings given in this section were carried out. The studies were run using a Tesla K80 GPU with 12 GB of NVIDIA RAM, which can run for up to 12 hours.

For the tests, a variety of libraries like Sklearn, numpy, Tensorflow, and Matplotlib were used. The Adam optimizer was utilized, with an initial learning rate of 0.002, and a dynamic learning rate method was used during training, where the learning rate was decreased using the ReduceLROnPlateau methodology when the improvement phase came to an end. Different parameter values, such as a factor of 0.5, patience of 10, and a minimal learning rate of 10-3, were used in the studies. The training phase was terminated if the validation loss did not decrease for 10 consecutive epochs using an early stopping strategy with a patience of 10.The models were trained for about 20 minutes, and the experiments were run for a total of 30 epochs with a batch size of 64. Multi-class classification was required for the task, and the output layer used softmax activation with categorical cross-entropy as the loss function. Let's now talk about image normalization, data augmentation, and data preprocessing. Data preparation is done to aid training by enhancing the images' visual capabilities. Enhancing contrast, removing high/low spatial frequency components, and lowering noisy components in the images are some of the aspects that might help improve visual ability. Two primary preprocessing methods are used in this paper. As is typical in many deep learning models for image classification applications, the photos are first resized to 224 by 224 pixels. Additionally, using the "min-max normalisation" technique, intensity normalisation is carried out to normalise the intensity of the picture pixels from their original 0-255 values to a normal distribution, which aids in removing bias and achieving a uniform distribution. This consistency can hasten the ORSAN algorithm's convergence, the model employed in this study [1]. During the model's training, data augmentation is also used. By applying multiple alterations to the original photos, new training examples are created through data augmentation, increasing the variety of images available for training. This enhances the model's overall performance and increases its capacity to generalise to new data. The resilience of the model during training can be increased by using data augmentation techniques like rotation, flipping, and zooming to obtain more training samples. Padding, horizontal flipping, and cropping are a few of the augmentation techniques used in this work to address overfitting problems in the data. The suggested ORSAN model makes use of transfer learning, which includes applying previously learned characteristics from a base model that has already been trained to a target model. This is regarded as an optimisation strategy that can improve performance while saving time

and resources. Transfer learning is especially helpful when the features discovered from the training dataset can be applied to the target dataset as well as the training job. In feature extraction, fixed features are eliminated, and the model is trained using data from the middle layer. In fine-tuning, the pre-trained model is further trained using the target data. In this work, ORSAN replaces the fully connected layer at the end and takes into account the dense and regularisation layers in addition to the pre-trained weights of ResNet 50, ResNet 101, and ResNet 152. Our ORSAN model's primary goal is to identify and assess coronavirus infection. The information is divided into groups for normal lung, COVID-19-infected lung, and pneumonia. A 3x3 confusion matrix is used to assess the model's performance and offers information on the model's classification accuracy and misclassification rates. Calculated was the three-level classification's detection rate, which took into account true positives, false positives, true negatives, and false negatives. These numbers shed light on the model's precision in recognising lung infection patients and the frequency of misclassifications. Multiple lungs might be impacted in some circumstances, but the model might falsely claim that they are not. When analysing our data, our ORSAN model outperformed conventional methods and conventional ResNet techniques. Despite severe memory limitations, we were able to calculate results rapidly and precisely thanks to the Adam optimizer. The findings of ResNet50 are shown in Table 3, which had an overall accuracy of 87.19%, an accuracy of 98.32% for COVID-19 detection, and accuracy of 87.28% and 88.8% for pneumonia and healthy lungs, respectively.

Class	Precision	Recall	F1-Score	Accuracy
Normal	0.87	0.86	0.76	88.80%
Pneumonia	0.90	0.92	0.91	87.28%
COVID-19	0.10	0.50	0.17	98.32%

Table3. Performance evaluation of ResNet50

Class	Precision	Recall	F1-Score	Accuracy
Normal	0.81	0.85	0.83	90.66%
Pneumonia	0.94	0.92	0.93	90.15%
COVID-19	0.44	0.89	0.59	97.99%

Table 4.Performance evaluation of ORSAN

Table 5. Performance evaluation of ResNet152

Class	Precision	Recall	F1-Score	Accuracy
Normal	0.62	0.73	0.67	83.68%
Pneumonia	0.91	0.85	0.88	82.00%
COVID-19	0.10	0.50	0.17	98.32%

The evaluation results of ORSAN are shown in Table 4, with a COVID-19 accuracy rate of 98.74% and accuracies for normal lungs and lungs damaged by pneumonia of 92.08% and 91.32%, respectively. Table 5 demonstrates that ResNet152 obtained accuracy for normal lungs and lungs affected by pneumonia of 83.68% and 82%, respectively, with an overall accuracy of 82%. The recall and precision curves of ResNet50, ORSAN, and ResNet152 with respect to epochs are shown in Figures 2 and 3. To get the ResNet models' peak values, we ran 30 epochs. Infection with COVID-19, pneumonia, and healthy lungs had ResNet50 recall ratings of 50%, 92%, and 87%, respectively. With regard to the COVID-19 infection, pneumonia infection, and healthy lungs, ResNet101 attained recall values of 86%, 92%, and 87%, respectively. For pneumonia, ResNet152 recorded a recall rating of 85%.

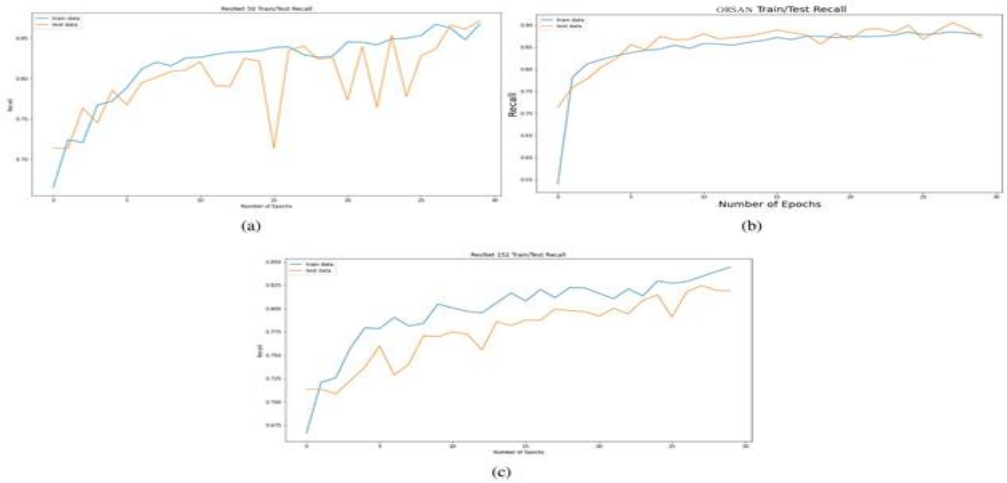

Fig. 2. Recall curve on the basis of 30 epochs for (a) ResNet50, (b) ORSAN, (c) ResNet152

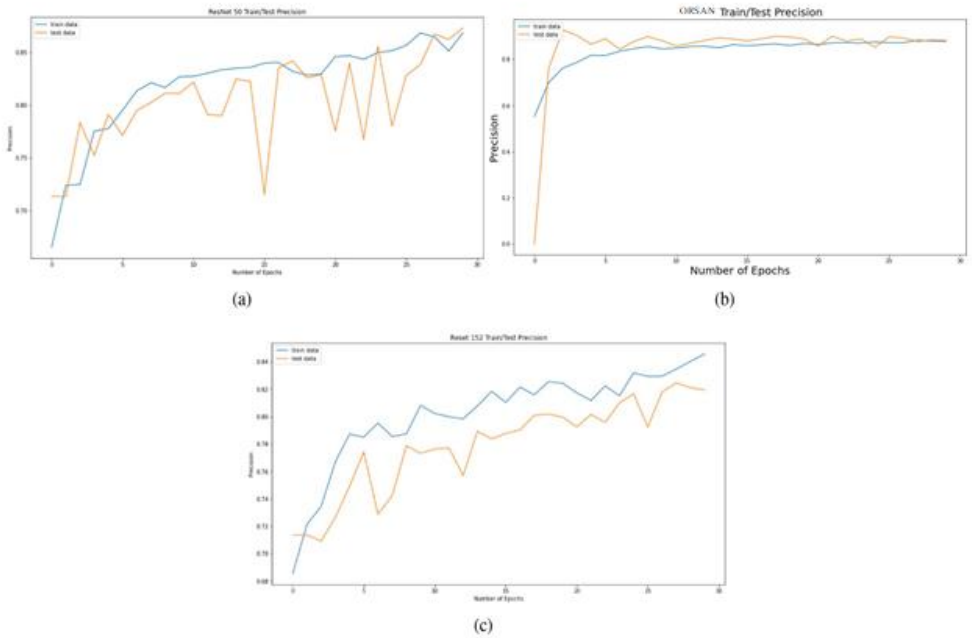

Fig. 3. AUC curve on the basis of 30 epochs for (a) ResNet50, (b) ORSAN, (c) ResNet152.

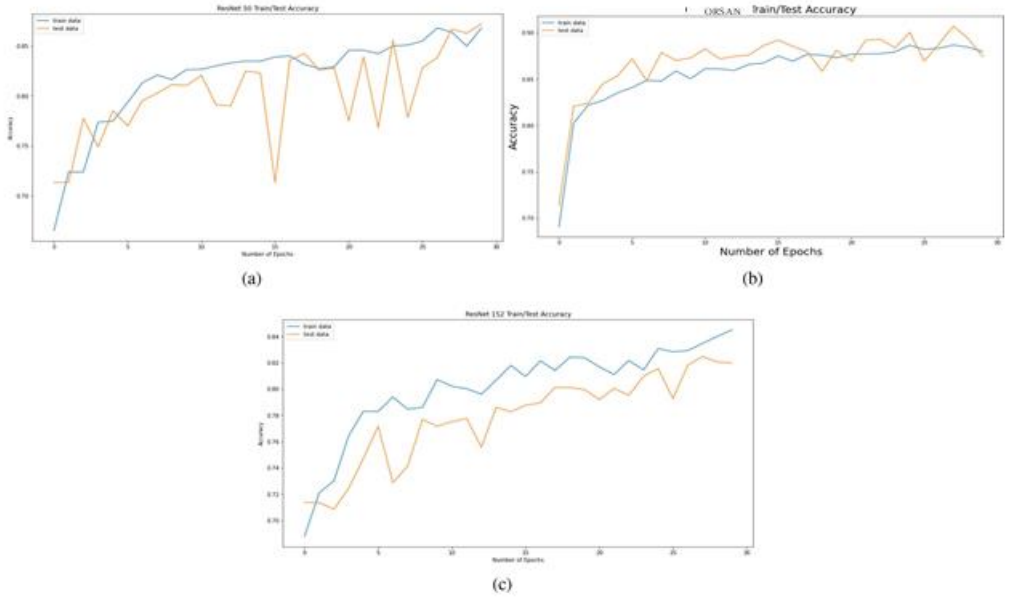

Fig. 4 Accuracy curve on the basis of 30 epochs for (a) ResNet50, (b) ORSAN (c) ResNet152.

Figure 4 illustrates the model's performance during training by displaying the AUC values for the training and testing states for each epoch. The accuracy curve for 30 epochs is also shown in Figure 5, which enables us to deduce the peak value from the curve. Similar to Figure 9, Figure 10 shows the loss curves for various ResNet models and demonstrates how the losses reduce with increasing epochs, indicating more accurate findings with lower loss values.

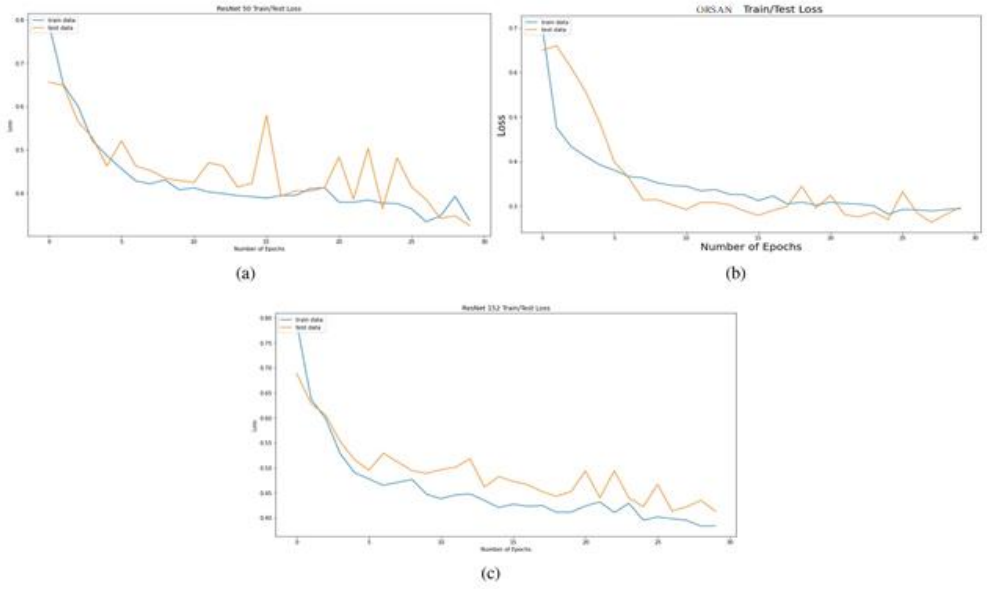

Fig. 5. Losses of model based on 30 epochs for (a) ResNet50, (b) ORSAN(c) ResNet152.

Figures 6–8 show the ROC curves, where "0" denotes healthy lungs, "1" denotes lungs damaged by pneumonia, and "2" denotes lungs impacted by SARS-CoV-2. Figure 11 shows that the ROC values for healthy lungs, lungs damaged by pneumonia, and lungs affected by COVID-19 are 95%, 93%, and

88%, respectively. Additionally, Figure 12 shows that the ROC values for healthy lungs, lungs affected by pneumonia, and lungs affected by COVID-19 are 96%, 95%, and 97%, respectively.

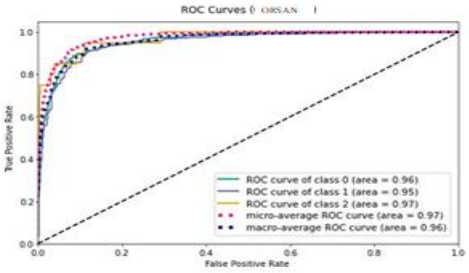

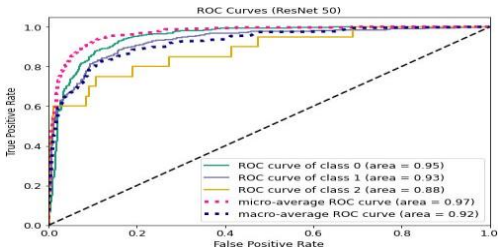

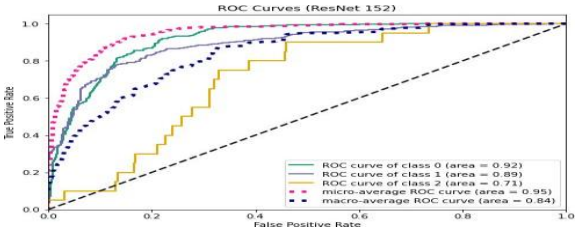

In addition, ResNet152 obtained a ROC value of 71% for lungs afflicted by COVID-19, as demonstrated in Figure 13. Additionally, we contrasted our ORSAN model with conventional ResNet models. Other current algorithms, such as ResNet50 and ResNet152, performed worse than our ORSAN. The literature covered earlier studies on COVID-19 categorization using X-ray imaging. For instance, binary classification was the focus of the work of [35] and [61]. For Xception and Inception, [35] attained an accuracy of 80%.Individually, ResNetV2 models provided accuracy of 90.55%, while [61] published results for the VGG 16 model with Adam and RMSprop optimizers. However, [35] and [61] only used a small number of images, as opposed to our proposed work, which made use of a larger dataset of 5,935 X-ray images. Additionally, [59] and [60] performed a three-level classification that included COVID-19, pneumonia, and healthy lungs. ResNet34 attained a precision of 88.4% in [59], but our suggested ORSAN attained a precision of 90.20%. In addition, MobileNetV2 attained an accuracy of 90% for three-level classification in the work of [60], whereas our ORSAN achieved an accuracy of 90.90% for the same classification assignment.

6. Conclusion

For the multiclass classification of lung infections, including pneumonia and COVID-19, this study suggests a unique ORSAN method. The evaluation was carried out for healthy lungs, lungs damaged by pneumonia, and lungs impacted by COVID-19 utilising a dataset made up of 5,935 pictures that were taken from two distinct databases. Other conventional ResNet models were outperformed by the ORSAN algorithm, which is an optimised version of ResNet101 obtained through hyperparameter tuning. Using ResNet101, it was discovered that the detection rate for COVID-19 was 98.74%, but the detection accuracies for normal lungs and lungs damaged by pneumonia were 92.08% and 91.32%, respectively. ResNet152, in contrast, attained detection accuracies of 83.68% for healthy lungs and 82% for lungs affected by pneumonia.

References

[1] J.Singh,B.K.Sharma,Novel approach for Object Recognition using Self Attention Networks: ORSAN

[2] T.P. Velavan and C.G. Meyer, The COVID-19 epidemic, Tropical Medicine & International Health 25(3) (2020), 278.

[3] B. Pfefferbaum and C.S. North, Mental health and the Covid19 pandemic, New England Journal of Medicine 383(6) (2020), 510–512.

[4] A. Carfí, R. Bernabei and F. Landi, Persistent symptoms in patients after acute COVID-19, Jama 324(6) (2020), 603–605.

[5] M.E. Chowdhury, T. Rahman, A. Khandakar, R. Mazhar, M.A. Kadir, Z.B. Mahbub, K.R. Islam, M.S. Khan, A. Iqbal, N. Al Emadi and M.B. Reaz, Can AI help in screening viral and COVID-19 pneumonia, IEEE Access 2020, pp. 132665– 132676.

[6] S. Bharati, P. Podder and M.R.H. Mondal, Hybrid deep learning for detecting lung diseases from X-

ray images, Informatics in Medicine Unlocked 20 (2020), 100391. doi: 10.1016/j.imu. 2020.100391.
[7] R.M. Pereira, D. Bertolini, L.O. Teixeira, C.N. Silla, Jr and Y.M. Costa, COVID-19 identification in chest X-ray images on flat and hierarchical classification scenarios, Computer Methods and Programs in Biomedicine 194 (2020), 105532.
[8] M.R.H. Mondal, S. Bharati, P. Podder and P. Podder, Data analytics for novel coronavirus disease, Informatics in Medicine Unlocked 20 (2020), 100374.
[9] S. Xu and Y. Li, Beware of the second wave of COVID-19, The Lancet 395(10233) (2020), 1321–1322.
[10] K. Leung, J.T. Wu, D. Liu and G.M. Leung, First-wave COVID-19 transmissibility and severity in China outside Hubei after control measures, and second-wave scenario planning: A modelling impact assessment, The Lancet 395(10233) (2020), 1382–1393.
[11] H. Alghamdi, G. Amoudi, S. Elhag, K. Saeedi and J. Nasser, Deep learning approaches for detecting COVID-19 from chest X-ray images: A Survey, IEEE Access 2021. 84 S. Bharati et al. / CO-ResNet: Optimized ResNet model for COVID-19 diagnosis from X-ray images
[12] L. Chang, W. Hou, L. Zhao, Y. Zhang, Y. Wang, L. Wu, T. Xu, L. Wang, J. Wang, J. Ma and L. Wang, The prevalence of antibodies to SARS-CoV-2 among blood donors in China, Nature Communications 12(1) (2021).
[13] J.L. He, L. Luo, Z.D. Luo, J.X. Lyu, M.Y. Ng, X.P. Shen and Z. Wen, Diagnostic performance between CT and initial realtime RT-PCR for clinically suspected 2019 coronavirus disease (COVID-19) patients outside Wuhan, China, Respiratory Medicine 168 (2020), 105980.
[14] R. Mardani, A.A. Vasmehjani, F. Zali, A. Gholami, S.D. Nasab, H. Kaghazian, M. Kaviani and N. Ahmadi, Laboratory parameters in detection of COVID-19 patients with positive RT-PCR; a diagnostic accuracy study, Archives of Academic Emergency Medicine 8(1) (2020).
[15] H.Y. Wong, H.Y. Lam, A.H. Fong, S.T. Leung, T.W. Chin, C.S. Lo, M.M. Lui, J.C. Lee, K.W. Chiu, T.W. Chung and E.Y. Lee, Frequency and distribution of chest radiographic findings in patients positive for COVID-19, Radiology 296(2) (2020), E72–E78.
[16] S.H. Yoon, K.H. Lee, J.Y. Kim, Y.K. Lee, H. Ko, K.H. Kim, C.M. Park and Y.H. Kim, Chest radiographic and CT findings of the 2019 novel coronavirus disease (COVID-19): Analysis of nine patients treated in Korea, Korean Journal of Radiology 21(4) (2020).
[17] X. Xie, Z. Zhong, W. Zhao, C. Zheng, F. Wang and J. Liu, Chest CT for typical coronavirus disease 2019 (COVID-19) pneumonia: Relationship to negative RT-PCR testing, Radiology 296(2) (2020), E41–E45.
[18] Y. Fang, H. Zhang, J. Xie, M. Lin, L. Ying, P. Pang and W. Ji, Sensitivity of chest CT for COVID-19: Comparison to RTPCR, Radiology 296(2) (2020), E115–E117.
[19] J.F. Chan, S. Yuan, K.H. Kok, K.K. To, H. Chu, J. Yang, F. Xing, J. Liu, C.C. Yip, R.W. Poon and H.W. Tsoi, A familial cluster of pneumonia associated with the 2019 novel coronavirus indicating person-to-person transmission: A study of a family cluster, The Lancet 395(10223) (2020), 514–523.
[20] T. Ai, Z. Yang, H. Hou, C. Zhan, C. Chen, W. Lv, Q. Tao, Z. Sun and L. Xia, Correlation of chest CT and RT-PCR testing for coronavirus disease 2019 (COVID-19) in China: A report of 1014 cases, Radiology 296(2) (2020), E32–E40.
[21] S. Latif, M. Usman, S. Manzoor, W. Iqbal, J. Qadir, G. Tyson, I. Castro, A. Razi, M.N. Boulos, A. Weller and J. Crowcroft, Leveraging data science to combat covid-19: A comprehensive review, IEEE Transactions on Artificial Intelligence 2020.
[22] L. Wynants, B. Van Calster, G.S. Collins, R.D. Riley, G. Heinze, E. Schuit, M.M. Bonten, D.L. Dahly, J.A. Damen, T.P. Debray and V.M. de Jong, Prediction models for diagnosis and prognosis of covid-19: Systematic review and critical appraisal, BMJ 2020.
[23] H. Swapnarekha, H.S. Behera, J. Nayak and B. Naik, Role of intelligent computing in COVID-19 prognosis: A state-of-theart review, Chaos, Solitons & Fractals 138 (2020), 109947.
[24] S. Bharati and P. Podder, 1 Performance of CNN for predicting cancerous lung nodules using LightGBM, in: Artificial Intelligence for Data-Driven Medical Diagnosis, De Gruyter 2021, pp. 1–18. [25] S. Bharati, P. Podder and M.R.H. Mondal, Artificial neural network based breast cancer screening: A comprehensive review, International Journal of

Computer Information Systems and Industrial Management Applications 12 (2020), 125–137.
[26] A. Khamparia, S. Bharati, P. Podder, D. Gupta, A. Khanna, T.K. Phung and D.N.H. Thanh, Diagnosis of breast cancer based on modern mammography using hybrid transfer learning, Multidimensional Systems and Signal Processing 32(2) (2021), 747–765.
[27] A. Adegun and S. Viriri, Deep learning techniques for skin lesion analysis and melanoma cancer detection: A survey of state-of-the-art, Artificial Intelligence Review 54(2) (2021), 811–841.
[28] Y. Jiang, X. Liang, X. Wang, C. Chen, Q. Yuan, X. Zhang, N. Li, H. Chen, J. Yu, Y. Xie and Y. Xu, Noninvasive prediction of occult peritoneal metastasis in gastric cancer using deep learning, JAMA Network Open 4(1) (2021), e2032269.
[29] M. Kim and B.D. Lee, Automatic lung segmentation on chest X-rays using self-attention deep neural network, Sensors 21(2) (2021), 369.
[30] J.C. Souza, J.O. Diniz, J.L. Ferreira, G.L. da Silva, A.C. Silva and A.C. de Paiva, An automatic method for lung segmentation and reconstruction in chest X-ray using deep neural networks, Computer Methods and Programs in Biomedicine 177 (2019), 285–296.
[31] P. Lakhani and B. Sundaram, Deep learning at chest radiography: Automated classification of pulmonary tuberculosis by using convolutional neural networks, Radiology 284(2) (2017), 574–582. [32] P. Rajpurkar, J. Irvin, K. Zhu, B. Yang, H. Mehta, T. Duan, D. Ding, A. Bagul, C. Langlotz, K. Shpanskaya and M.P. Lungren, Chexnet: Radiologist-level pneumonia detection on chest x-rays with deep learning, arXiv preprint 2017, arXiv: 1711.05225.
[33] D. Dong, Z. Tang, S. Wang, H. Hui, L. Gong, Y. Lu, Z. Xue, H. Liao, F. Chen, F. Yang and R. Jin, The role of imaging in the detection and management of COVID-19: A review, IEEE Reviews in Biomedical Engineering 2020.
[34] S. Bharati, P. Podder, M.R.H. Mondal and N. Gandhi, Optimized NASNet for Diagnosis of COVID-19 from Lung CT Images, in: Intelligent Systems Design and Applications (ISDA 2020), A. Abraham, V. Piuri, N. Gandhi, P. Siarry, A. Kaklauskas, A. Madureira, eds, Advances in Intelligent Systems and Computing, Springer, Cham 1351 (2021), 647–656. doi: 10.1007/978-3-030-71187-0_59.
[35] E.E. Hemdan, M.A. Shouman and M.E. Karar, Covidx-net: A framework of deep learning classifiers to diagnose covid-19 in x-ray images, arXiv preprint 2020 arXiv: 2003.11055.
[36] J.P. Cohen, P. Morrison and L. Dao, COVID-19 Image Data Collection, arXiv 2020, arXiv: 2003.11597v1.
[37] Detecting COVID-19 in X-ray Images with Keras, TensorFlow, and Deep Learning. Available online: https://www.pyimagesearch.com/2020/03/16/detecting-covid-19-in-x-ray-imageswith-keras-tensorflowand-deep-learning/ (accessed on 16 June 2020).
[38] L. Wang and A. Wong, COVID-Net: A Tailored Deep Convolutional Neural Network Design for Detection of COVID-19 Cases from Chest X-ray Images. arXiv 2020, arXiv: 2003. 09871.
[39] COVID-19 Chest X-ray Dataset Initiative. Available online: https://github.com/agchung/Figure1-COVIDchestxraydataset (accessed on 16 June 2020).
[40] RSNA Pneumonia Detection Challenge. Available online: https://www.kaggle.com/c/rsna-pneumoniadetection-challenge/data (accessed on 16 June 2020).
[41] Actualmed-COVID-chestxray-dataset. Available online: https: //github.com/agchung/Actualmed-COVIDchestxray-dataset (accessed on 16 June 2020).
[42] COVID-19 Radiography Database. Available online: https:// www.kaggle.com/tawsifurrahman/covid19-radiographydatabase (accessed on 16 June 2020). S. Bharati et al. / CO-ResNet: Optimized ResNet model for COVID-19 diagnosis from X-ray images 85 [43] I.D. Apostolopoulos and T.A. Mpesiana, Covid-19: Automatic detection from X-ray images utilizing transfer learning with convolutional neural networks, Phys Eng Sci Med 43 (2020), 635–640.
[44] Italian Society of Medical and Interventional Radiology (SIRM). Available online: https://www.sirm.org/en/italiansociety-of-medical-and-interventional-radiology/ (accessed on 16 June 2020).

[45] Radiopaedia. Available online: https://radiopaedia.org/ (accessed on 16 June 2020).
[46] P. Kumar and S. Kumari, Detection of coronavirus Disease (COVID-19) based on Deep Features, Preprints 2020.
[47] Chest X-ray Images (Pneumonia). Available online: https:// www.kaggle.com/paultimothymooney/chestxray-pneumonia (accessed on 16 June 2020).
[48] T. Ozturk, M. Talo, E.A. Yildirim, U.B. Baloglu, O. Yildirim and U.R. Acharya, Automated detection of COVID-19 cases using deep neural networks with X-ray images, Comput Biol Med 121 (2020), 103792.
[49] X. Wang, Y. Peng, L. Lu, Z. Lu, M. Bagheri and R.M. Summers, ChestX-ray8: Hospital-scale chest X-ray database and benchmarks on weakly-supervised classification and localization of common thorax diseases, in: Proceedings of the 2017 IEEE Conference on Computer Vision and Pattern Recognition (CVPR) 2017, pp. 3462–3471.
[50] https://www.kaggle.com/andrewmvd/convid19-x-rays (accessed on 16 April 2021).
[51] K. He, X. Zhang, S. Ren and J. Sun, Deep residual learning for image recognition, in: Proceedings of the IEEE Conference on Computer Vision and Pattern Recognition 2016, pp. 770–778.
[52] T. Rahman, A. Khandakar, Y. Qiblawey et al., Exploring the effect of image enhancement techniques on COVID-19 detection using chest X-ray images, Computers in Biology and Medicine 132 (2021), 104319.
[53] H. Panwar, P.K. Gupta, M.K. Siddiqui, R. Morales-Menendez and V. Singh, Application of deep learning for fast detection of COVID-19 in X-Rays using nCOVnet, Chaos, Solitons & Fractals 138 (2020), 109944.
[54] F. Ucar and D. Korkmaz, COVIDiagnosis-Net: Deep BayesSqueezeNet based diagnosis of the coronavirus disease 2019 (COVID-19) from X-ray images, Medical Hypotheses 140 (2020), 109761.
[55] A.A. Hussain, O. Bouachir, F. Al-Turjman and M. Aloqaily, AI techniques for COVID-19, IEEE Access 8 (2020), 128776– 128795.
[56] D.P. Kingma and J. Ba, Adam: A method for stochastic optimization, arXiv preprint 2014, arXiv: 1412.6980.
[57] I. Sutskever, J. Martens, G. Dahl and G. Hinton, On the importance of initialization and momentum in deep learning, in: International Conference on Machine Learning, 2013, pp. 1139–1147.
[58] M.D. Zeiler, Adadelta: An adaptive learning rate method, arXiv preprint 2012, arXiv: 1212.5701. [59] M.R. Karim, T. Döhmen, M. Cochez, O. Beyan, D. RebholzSchuhmann and S. Decker, Deep COVID explainer: explainable COVID-19 diagnosis from chest X-ray images, 2020 IEEE International Conference on Bioinformatics and Biomedicine (BIBM) 2020, pp. 1034–1037, doi: 10.1109/BIBM49941.2020. 9313304.
[60] E. Luz, P. Silva, R. Silva, L. Silva, J. Guimarães, G. Miozzo, G. Moreira and D. Menotti, Towards an effective and efficient deep learning model for covid-19 patterns detection in X-ray images, Research on Biomedical Engineering 2021, pp. 1–14.
[61] H. Swapnarekha, H.S. Behera, D. Roy, S. Das and J. Nayak, Competitive deep learning methods for COVID-19 detection using X-ray images, Journal of The Institution of Engineers (India): Series B 2021. doi: 10.1007/s40031-021-00589-3.
[62] P. Podder, S. Bharati, M.R.H. Mondal and U. Kose, Application of machine learning for the diagnosis of COVID-19, Data Science for COVID-19 2021, pp. 175–194, Academic Press. doi: 10.1016/B978-0-12-824536-1.00008-3.
[63] P. Podder, S. Bharati, M.A. Rahman and U. Kose, Transfer learning for classification of brain tumor, Deep Learning for Biomedical Applications 2021.
[64] P. Podder, A. Khamparia, M.R.H. Mondal, M.A. Rahman and S. Bharati, Forecasting the spread of COVID-19 and ICU requirements, International Journal of Online and Biomedical Engineering (iJOE) 17(5) (2021), 81–99. doi: 10.3991/ijoe. v17i05.20009.
[65] H. Chen, Y. Zhang, M.K. Kalra, F. Lin, Y. Chen, P. Liao, J. Zhou and G. Wang, Low-dose CT with a residual encoderdecoder convolutional neural network, IEEE Transactions on Medical Imaging 36(12) 2017, pp. 2524–2535.
[66] S. Bharati, P. Podder and M.R.H. Mondal, X-ray images three levels, Figshare 2021, doi: 10.6084/m9.figshare.14755965. v1